

Resolution of small-angle neutron scattering with a reflective focusing optic

David F. R. Mildner

NIST Center for Neutron Research, National Institute of Standards and Technology, 100 Bureau Drive, Gaithersburg, MD 20899, USA. Correspondence e-mail: david.mildner@nist.gov

A small-angle neutron scattering instrument that uses a reflective focusing optic can achieve smaller values of the scattering vector, and with higher resolution, than the usual pinhole collimation. When the focusing mirror images the source onto the detector, the analytic expression for the resolution is independent of the sample area and is principally determined by the beam divergence incident on the sample, modified by the distance between the optic and the sample. The results are applied to a focusing SANS instrument with axisymmetric mirrors.

1. Introduction

Small-angle neutron scattering (SANS) is usually performed on a pinhole instrument, for which two circular (or rectangular) apertures placed a large distance apart define the neutron beam with the necessary narrow divergence incident on the sample. The optimum configuration to obtain the maximum count rate for a given resolution is with the source aperture radius twice that of the sample and with the two-dimensional detector at a distance beyond the sample aperture equal to the source–sample distance. This configuration defines a minimum scattering vector magnitude Q_{\min} available for the instrument for a given wavelength [$Q = (4\pi/\lambda)\sin(\theta/2)$, where θ is the scattering angle and λ is the wavelength of the incident radiation].

Various methods have been proposed to focus the incident beam onto the detector so that the direct-beam profile at the detector is less broad and closer to a unit function. This enables a reduction in the value of Q_{\min} , an improvement in the resolution of the measurement and an increase in the neutron flux on the sample. These methods include using refractive and reflective optics and magnetic focusing. A compound refractive lens composed of multiple spherical biconcave MgF_2 lenses has been used successfully to focus a cold neutron beam (Eskildsen *et al.*, 1998; Choi *et al.*, 2000; Frielinghaus *et al.*, 2009). High-resolution focusing SANS is also performed using grazing incidence with a single toroidal mirror as the reflective optic (Alefild *et al.*, 1989; Goerigk & Varga, 2011). More recently, Liu *et al.* (2013) have demonstrated a novel method for focusing a neutron beam with axisymmetric mirrors that might be useful for small-angle scattering.

If the detector is placed at the image position of the source with respect to the optic, the beam size is independent of the size of the sample for both refractive and reflective optics. This results in a reduction in the value of Q_{\min} and an improved resolution in the measurement. A refractive optic is strongly chromatic and is only beneficial with beams that have a relatively narrow wavelength spread. It may have only limited use

for time-of-flight measurements, where the longest wavelengths, which contribute to the smallest Q values, may be separated from the out-of-focus beams by time of flight. On the other hand, a reflective optic is achromatic, but a single-reflection mirror system has increased aberration, principally from coma, as exemplified by an elliptic mirror system (Bentley *et al.*, 2012).

The difficulty with grazing-incidence optics is that a near-parallel incident beam is required, and so the optical element must be placed far enough from the source to ensure a small incident-beam divergence. Kirkpatrick–Baez neutron mirrors (Ice *et al.*, 2005) using two successive reflections in orthogonal directions can efficiently focus neutron beams onto a small area, with a maximum divergence that is limited by the critical angle of the mirror. The size of the focal spot is primarily determined by the geometric demagnification of the source and by figure errors in the mirror shape.

Grazing-angle reflection optics based on the Wolter (1952) mirror geometry are used extensively in X-ray astronomy (Joy,

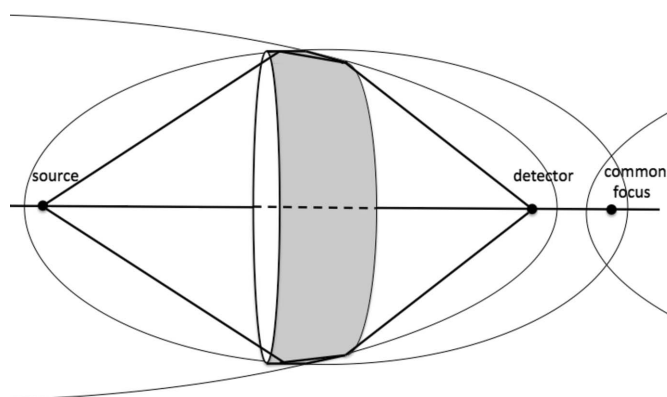


Figure 1
A schematic diagram of the Wolter optics of the confocal ellipsoid and hyperboloid mirror system used by Liu *et al.* (2013). The source is located at the focus of the ellipsoid and the detector is placed at the focus of the hyperboloid, with the other focus of each being coincident. Only one mirror is shown.

2001), as two reflections minimize both coma and optical aberrations for off-axis trajectories. Mildner & Gubarev (2011) discussed the opportunity of Wolter optics designs to eliminate the aberration of coma for focusing of cold and thermal neutron beams, using two consecutive reflections from different conic surfaces of revolution, such as parabolic and hyperbolic surfaces. Fig. 1 shows the elliptic–hyperbolic mirror system used by Liu *et al.* (2013). Multiple axisymmetric mirrors, having different diameters but the same focal length, may be combined by nesting inside each other to increase the useful beam area and therefore the incident-beam intensity. Liu *et al.* (2012) discussed the various factors associated with beam divergence and the efficiency of neutron collection for such nested mirrors.

The geometric resolution of a simple pinhole instrument has been determined (Mildner & Carpenter, 1984) in terms of the sizes of the two apertures and the detector element and the distances between them. This has been adapted for a SANS instrument with refractive optics (Mildner, 2005), where the focusing of the incident beam involves correlations between the source and sample apertures, resulting in a great relaxation of the limits on sample size. We now apply the same procedure to a SANS configuration that involves reflective optics.

2. Resolution of the focusing optic

Let the vectors \mathbf{r}_1 , \mathbf{r}_2 and \mathbf{r}_D represent general points on the effective source plane, on the sample plane and on the detector plane, respectively. For a simple pinhole SANS instrument, the usual assumption is that there is no correlation between points on the source and sample areas and detector elements, so that averages over all points within the three areas are independent of each other. The mean positions of these distributions define the mean directions, $\mathbf{\Omega}_1$ and $\mathbf{\Omega}_2$, of the incident and scattered neutrons, respectively, so that the scattering angle θ is given by $\cos \theta = \mathbf{\Omega}_1 \cdot \mathbf{\Omega}_2$. The variance σ_Q of the magnitude of the scattering vector $|\mathbf{Q}|$ at small scattering angles θ is given (Mildner & Carpenter, 1984) by

$$(\sigma_Q)^2 = \frac{k^2}{\sin^2 \theta} \left[\frac{\langle (\mathbf{r}_1 \cdot \mathbf{\Omega}_2)^2 \rangle}{L_1^2} + \frac{\langle (\mathbf{r}_2 \cdot \mathbf{\Omega}_2)^2 \rangle}{L'^2} + \frac{\langle (\mathbf{r}_D \cdot \mathbf{\Omega}_2)^2 \rangle}{L_2^2} \right], \quad (1)$$

where the scattering vector magnitude $Q = k\theta$ at small angles, with the neutron wavevector $k = 2\pi/\lambda$ and the wavelength λ . L_1 and L_2 are the incident (source-to-sample) and scattered (sample-to-detector) path lengths, respectively, and the reduced path length is given by

$$\frac{1}{L'} = \frac{1}{L_1} + \frac{1}{L_2}. \quad (2)$$

The angle brackets $\langle \dots \rangle$ denote averages over all points within the area of the source, sample or detector element. This is valid for azimuthally symmetric scattering such that the data can be radially averaged.

We analyze the reflection focusing optic as if it were a perfect simple converging optic. Fig. 2 shows the axially symmetric arrangement for a single reflective optic or cylindrical mirror, such that the size of the image depends on

the source size and the ratio of the distances from the mirror. The sample plane is located at a distance L_O after the optic center, such that the source is a distance $(L_1 - L_O)$ before the mirror plane and the detector plane is at a distance $(L_2 + L_O)$ after the mirror plane. If these are conjugate distances for the focal length f of the mirror, given by

$$\frac{1}{f} = \frac{1}{L_1 - L_O} + \frac{1}{L_2 + L_O}, \quad (3)$$

then the mirror system has a magnification of $(L_2 + L_O)/(L_1 - L_O)$. That is, the radius of the beam profile at the detector is given by the mirror equation as $R_1(L_2 + L_O)/(L_1 - L_O)$, where R_1 is the radius of the source.

For any focusing SANS configuration, a trajectory direction incident on the sample is defined by the focusing optic and the point of convergence, such that the distributions that define the source and the sample are not independent. This means that there is a correlation between points within the areas that define both the source and the sample, and this ultimately defines the incident-beam resolution. Consequently, the analysis of the resolution for the focusing mirror optic needs to take into account the correlations between a typical point \mathbf{r}_1 on the effective source plane and a point \mathbf{r}_2 on the sample plane, though not also with the detector element points \mathbf{r}_D . In this case, the variance of the magnitude of the scattering vector is

$$(\sigma_Q)^2 = \frac{k^2}{\sin^2 \theta} \left[\left\langle \left(\frac{\mathbf{r}_1 \cdot \mathbf{\Omega}_2}{L_1} - \frac{\mathbf{r}_2 \cdot \mathbf{\Omega}_2}{L'} \right)^2 \right\rangle + \frac{\langle (\mathbf{r}_D \cdot \mathbf{\Omega}_2)^2 \rangle}{L_2^2} \right]. \quad (4)$$

In this analysis, we assume the optic is perfect so that we can ignore figure errors for the mirrors. The general points \mathbf{r}_O and \mathbf{r}_3 at the optic and within the transmitted beam at the detector define a trajectory that strikes the sample. Note that, since the optic–detector geometry defines the beam convergence onto

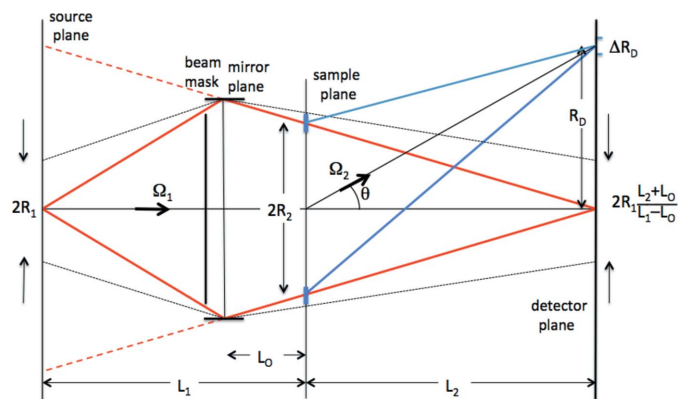


Figure 2 A schematic diagram of the general reflecting-mirror SANS geometry, with the source of aperture radius R_1 at a distance L_1 before the sample and the detector plane at a distance L_2 after the sample. The mirror is placed a distance L_O in front of the sample, such that the source is imaged at the detector, with the focusing geometry giving the beam profile a radius $R_1(L_2 + L_O)/(L_1 - L_O)$. A detector element ΔR_D is indicated at a distance R_D from the instrument axis, such that the scattering angle is given by $\sin \theta = R_D/L_2$. A beam stop is placed in front of the optic to eliminate rays that do not reflect from the mirror.

the sample, the effective source may be considered anywhere upstream of the optic or even at the optic itself. In Appendix A we consider the effective source to be located at the real source plane as in Fig. 3, though if we were to consider the effective source to be at the optic plane we would have the same result.

Averaging over points on the source and sample planes gives

$$\left\langle \left(\frac{\mathbf{r}_1 \cdot \boldsymbol{\Omega}_2}{L_1} - \frac{\mathbf{r}_2 \cdot \boldsymbol{\Omega}_2}{L'} \right)^2 \right\rangle = \left\langle \left(\frac{\mathbf{r}_3 \cdot \boldsymbol{\Omega}_2}{L_2} \right)^2 \right\rangle = \frac{\langle r_3^2 \rangle \sin^2 \theta}{2L_2^2}. \quad (5)$$

This result is independent of \mathbf{r}_O , which means that the variance of the scattering vector is independent of the size of the optic. This is not surprising, since the cross section of the optic only determines the instrument count rate and does not affect the resolution. This is determined by the size of the incident beam on the detector, which is related to the source size. However, the size of the optic is limited by the grazing-incidence angle for the mirror surface for a particular wavelength. Averaging over the beam spot at the detector gives

$$\langle r_3^2 \rangle = \frac{R_1^2}{2} \left(\frac{L_2 + L_O}{L_1 - L_O} \right)^2. \quad (6)$$

We also determine the average for data collected over a ring of width ΔR_D on the detector, corresponding to constant $|\mathbf{Q}|$. From equations (4) and (5), we obtain for the overall geometric contribution to the resolution

$$(\sigma_Q)^2 = k^2 \left(\frac{\langle r_3^2 \rangle}{2L_2^2} + \frac{\langle r_D^2 \rangle}{L_2^2} \right) = \frac{k^2}{L_2^2} \left[\frac{R_1^2}{4} \left(\frac{L_2 + L_O}{L_1 - L_O} \right)^2 + \frac{(\Delta R_D)^2}{12} \right]. \quad (7)$$

Note that this derivation assumes the simple mirror equation. Any length to the mirror results in aberration, such that the beam profile at the detector is no longer uniform. The uniform beam profile becomes an isosceles trapezoid of revolution for a mirror of length ℓ , resulting in an increased Q_{\min} . In addition,

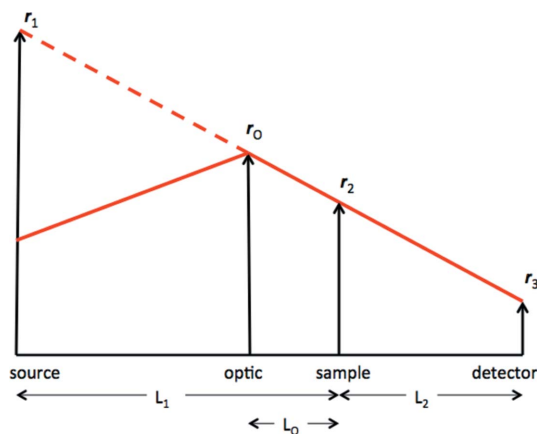


Figure 3
A schematic diagram depicting the construction of the (imaginary) vector \mathbf{r}_1 at the source plane for a general incident-beam trajectory that is defined by the vectors \mathbf{r}_O on the mirror plane and \mathbf{r}_3 on the detector plane. The trajectory also defines the vector \mathbf{r}_2 on the sample plane.

tion, the geometric resolution is increased by a second-order term in $(\ell/L'')^2$, with

$$\langle r_3^2 \rangle = \frac{R_1^2}{2} \left(\frac{L_2 + L_O}{L_1 - L_O} \right)^2 \left[1 + \frac{2}{3} \left(\frac{\ell}{L''} \right)^2 \right], \quad (8)$$

where

$$\frac{1}{L''} = \frac{1}{L_1 - L_O} + \frac{1}{L_2 + L_O}, \quad (9)$$

and $L'' = f$, the focal length of the mirror system. It is this extra term that goes to zero with the use of the double reflection of Wolter optics.

For greater resolution it is better to have a large distance between the optic and the detector, and for a fixed optic-detector distance the best resolution is obtained with the sample far from the detector and close to the optic. The price of any increase in L_O is a poorer Q_{\min} and resolution. If the sample were placed immediately behind the focusing mirror such that $L_O = 0$, the magnification would be L_2/L_1 and the geometric contribution to the resolution would reach a minimum of

$$(\sigma_Q)^2 = k^2 \left[\left(\frac{R_1}{2L_1} \right)^2 + \frac{1}{12} \left(\frac{\Delta R_D}{L_2} \right)^2 \right] \quad (10)$$

and be dominated by the beam divergence incident on the optic. It is not surprising that this result is, to the first order, the same as that for the refractive focusing lens when the sample is placed immediately after the lens. This means that the distance from the source to the optic principally determines the resolution. The advantage of reflective optics is that the focusing is achromatic; the disadvantage is the awkward annular geometry of the sample.

3. Nested Wolter optics

The result of calculating the resolution of reflective optics for a SANS instrument indicates that the diameter of the cylindrical mirror is immaterial, provided that all rays leaving from a point on the source plane are directed to the same point on the detector. This is achieved by Wolter optics (Wolter, 1952). Consequently, multiple cylinders of different radii can be nested inside each other in order to collect neutrons from a larger solid angle, thus increasing the neutron intensity on the sample without the resolution deteriorating.

We now apply the resolution results to a recent demonstration of a focusing SANS geometry with axisymmetric mirrors (Liu *et al.*, 2013). The optic was fabricated using an electroformed nickel replication process and consists of three nested coaxial confocal ellipsoids and hyperboloids. The length of the optic is 60 mm. Rays from the source, placed at one focus of the ellipsoid, undergo two reflections before converging to the focus of the hyperboloid.

For a focusing-mirror SANS instrument, the source aperture and the detector are placed at the two foci of the mirror system, with the sample placed at distances $L_O = 0.56$ m beyond the optic centerline and $L_2 = 0.08$ m before the

detector. We analyze the reflective focusing optic as if it were a perfect simple thin converging optic that is achromatic. The optic was placed such that the source–optic distance $L_1 - L_O = 2.56$ m and the optic–detector distance $L_2 + L_O = 0.64$ m. The magnification of the source radius R_1 is given by $(L_2 + L_O)/(L_1 - L_O) = \frac{1}{4}$. The source aperture has a diameter $2R_1 = 4$ mm, so the expected direct beam profile at the detector is 1 mm. This does not take into account any figure errors in the mirrors or any misalignment of the mirrors to each other or to the instrument axis. In practice, Liu *et al.* (2013) reported that the direct beam had an approximate Gaussian profile with a full width at half-maximum (FWHM) of 1.25 mm.

The second reflection (on the hyperboloid surface) defines the trajectory onto the sample, so that L_O becomes 0.545 m in equation (7) and the optic term in the resolution is $(R_1/2L_2)(L_2 + L_O)/(L_1 - L_O) = 3.03 \times 10^{-3}$. The detector is a 50 mm diameter microchannel plate with 48 μm pixels. The factor $(\Delta R_D/L_2)/(12)^{1/2} = 1.73 \times 10^{-4}$, so that the contribution of the high-resolution detector to the resolution is small. Hence, the overall resolution from angular contributions at the mean wavelength $\lambda = 7.8$ Å is $\sigma_Q = 2.44 \times 10^{-3}$ Å⁻¹. Liu *et al.* measured the instrumental resolution by time of flight over the wavelength range 6.4–9.2 Å. The wavelength contribution to the resolution is small, though it does increase linearly with scattering angle. The FWHM of the silver behenate Bragg peak at $Q_0 = 0.1078$ Å⁻¹ is given as $\Delta Q = 0.015$ Å⁻¹, resulting in $\sigma_Q = 6.4 \times 10^{-3}$ Å⁻¹.

Note that this analysis does not require the full 2π azimuthal symmetry of a cylindrical mirror; it can also apply to a high-resolution SANS instrument (Georigk & Varga, 2011) that uses a 1.2 m long by 0.12 m wide toroidal mirror coated with ⁶⁸Cu, as an approximation to an elliptical surface. In one configuration, the distances are $L_1 = 12.7$ m, $L_2 = 9.3$ m and $L_O = 1.7$ m, with the mirror length $\ell = 1.2$ m and the source size $2R_1 = 5$ mm. Equations (7) and (8) determine the optic contribution to the resolution to be $0.137 \times 10^{-3}k$, much larger than the detector (pixel size 0.365 mm) contribution of $0.011 \times 10^{-3}k$, where k is the neutron wavevector.

4. Conclusions

We have derived an analytical expression for the resolution of a small-angle scattering measurement on an instrument that uses a reflective focusing optic. There is a correlation between points on the source and sample areas that define those possible trajectories that can reach the image of the source at the detector. The analysis shows that the resolution depends principally on the source size and on the distances between the source, the reflecting optic, the sample position and the two-dimensional detector. Although the resolution does not depend on the sample size, the total count rate of the instrument does, so that gains in intensity are available for multiple mirrors without deterioration in the resolution.

This analysis has been applied to a recent demonstration of the capabilities of nested cylinders that employ a Wolter optics geometry for focusing neutrons onto the detector, though it also applies to more simple conic sections that do not cover

the full azimuthal angular range. The result is independent of the length of the optic.

Khaykovich *et al.* (2011) have proposed the use of Wolter optics not only for small-angle scattering but also for neutron imaging, with the mirrors placed between the sample and the detector.

APPENDIX A

Fig. 3 shows that points \mathbf{r}_1 on the effective source plane and \mathbf{r}_2 on the sample plane are related to points \mathbf{r}_3 on the detector plane and \mathbf{r}_O on the effective optic plane by

$$\frac{\mathbf{r}_1 - \mathbf{r}_3}{L_1 + L_2} = \frac{\mathbf{r}_O - \mathbf{r}_3}{L_O - L_2} = \frac{\mathbf{r}_2 - \mathbf{r}_3}{L_2}, \quad (11)$$

where L_1 is the distance from the source plane to the sample plane, L_2 is the distance from the sample plane to the detector plane, and L_O is the distance from the effective optic plane to the sample plane. Hence, we may write points \mathbf{r}_1 and \mathbf{r}_2 in terms of points \mathbf{r}_O and \mathbf{r}_3 , for which the distributions are independent of each other. That is,

$$\mathbf{r}_1 = \frac{L_1 + L_2}{L_O + L_2} \mathbf{r}_O + \frac{L_O - L_1}{L_O + L_2} \mathbf{r}_3, \quad (12)$$

$$\mathbf{r}_2 = \frac{L_2}{L_O + L_2} \mathbf{r}_O + \frac{L_O}{L_O + L_2} \mathbf{r}_3. \quad (13)$$

These results may be used to determine the variance of the scalar scattering vector by substitution into equation (4).

All planes are perpendicular to the incident-beam direction $\mathbf{\Omega}_1 = (1, 0, 0)$ and all points within these planes may be written $\mathbf{r} = (0, r\cos\varphi, r\sin\varphi)$, where φ is the azimuthal angle. The scattered neutron direction is given by $\mathbf{\Omega}_2 = (\cos\theta, \sin\theta\cos\varphi', \sin\theta\sin\varphi')$, where φ' is the azimuthal angle on the detector plane. Then for all \mathbf{r} , $\mathbf{r} \cdot \mathbf{\Omega}_2 = r\sin\theta\cos(\varphi - \varphi')$. Writing the contribution from the beam divergence to the overall resolution in terms of $\langle \mathbf{r}_O^2 \rangle$ and $\langle \mathbf{r}_3^2 \rangle$ for the optic cross-section and the transmitted beam profile at the detector, we find

$$\left\langle \left(\frac{\mathbf{r}_1 \cdot \mathbf{\Omega}_2}{L_1} - \frac{\mathbf{r}_2 \cdot \mathbf{\Omega}_2}{L'} \right)^2 \right\rangle = \left\langle \left(\frac{\mathbf{r}_3 \cdot \mathbf{\Omega}_2}{L_2} \right)^2 \right\rangle = \frac{\langle r_3^2 \rangle \sin^2 \theta}{2L_2^2}. \quad (14)$$

The factor of 2 comes from $\langle \cos^2(\varphi - \varphi') \rangle = \frac{1}{2}$.

This result is independent of r_O , which means that the variance of the scattering vector is independent of the size of the optic. Note that if we were to consider the effective source to be the optic plane, then we would have the same result, *viz.*

$$\left\langle \left(\frac{\mathbf{r}_O \cdot \mathbf{\Omega}_2}{L_O} - \frac{\mathbf{r}_2 \cdot \mathbf{\Omega}_2}{L''} \right)^2 \right\rangle = \left\langle \left(\frac{\mathbf{r}_3 \cdot \mathbf{\Omega}_2}{L_2} \right)^2 \right\rangle = \frac{\langle r_3^2 \rangle \sin^2 \theta}{2L_2^2}, \quad (15)$$

where $1/L'' = 1/L_O + 1/L_2$. Including the detector term, we obtain for the overall geometric resolution

$$(\sigma_Q)^2 = k^2 \left(\frac{\langle r_3^2 \rangle}{2L_2^2} + \frac{\langle r_D^2 \rangle}{L_2^2} \right). \quad (16)$$

Helpful discussions with J. G. Barker are acknowledged.

References

- Alefeld, B., Schwahn, D. & Springer, T. (1989). *Nucl. Instrum. Methods Phys. Res. Sect. A*, **274**, 210–216.
- Bentley, P. M., Kennedy, S. J., Andersen, K. H., Martín Rodríguez, D. & Mildner, D. F. R. (2012). *Nucl. Instrum. Methods Phys. Res. Sect. A*, **693**, 268–275.
- Choi, S.-M., Barker, J. G., Glinka, C. J., Cheng, Y. T. & Gammel, P. L. (2000). *J. Appl. Cryst.* **33**, 793–796.
- Eskildsen, M. R., Gammel, P. L., Issacs, E. D., Detlefs, C., Mortensen, K. & Bishop, D. J. (1998). *Nature*, **391**, 563–566.
- Frielinghaus, H., Pipich, V., Radulescu, A., Heiderich, M., Hanslik, R., Dahlhoff, K., Iwase, H., Koizumi, S. & Schwahn, D. (2009). *J. Appl. Cryst.* **42**, 681–690.
- Goerigk, G. & Varga, Z. (2011). *J. Appl. Cryst.* **44**, 337–342.
- Ice, G. E., Hubbard, C. R., Larson, B. C., Pang, J. W. L., Budai, J. D., Spooner, S. & Vogel, S. C. (2005). *Nucl. Instrum. Methods Phys. Res. Sect. A*, **539**, 312–320.
- Joy, M. K. (2001). *Astronomical X-ray Optics. Handbook of Optics*, Volume III, 2nd ed., edited by M. Bass, ch. 28. New York: McGraw Hill.
- Khaykovich, B., Gubarev, M. V., Bagdasarova, Y., Ramsey, B. D. & Moncton, D. E. (2011). *Nucl. Instrum. Methods Phys. Res. Sect. A*, **631**, 98–104.
- Liu, D., Gubarev, M. V., Resta, G., Ramsey, B. D., Moncton, D. E. & Khaykovich, B. (2012). *Nucl. Instrum. Methods Phys. Res. Sect. A*, **686**, 143–150.
- Liu, D., Khaykovich, B., Gubarev, M. V., Robertson, J. L., Crow, L., Ramsey, B. D. & Moncton, D. E. (2013). *Nat. Commun.* **4**, 2556.
- Mildner, D. F. R. (2005). *J. Appl. Cryst.* **38**, 488–492.
- Mildner, D. F. R. & Carpenter, J. M. (1984). *J. Appl. Cryst.* **17**, 249–256.
- Mildner, D. F. R. & Gubarev, M. V. (2011). *Nucl. Instrum. Methods Phys. Res. Sect. A*, **634**, S7–S11.
- Wolter, H. (1952). *Ann. Phys. (Leipzig)*, **445**, 94–114.